Bol. Soc. Paran. Mat.
©SPM – E-ISSN-2175-1188
SPM: www.spm.uem.br/bspm

(3s.) **v. 2026 (44) 7** : 1–17.
ISSN-0037-8712
doi:10.5269/bspm.80743

Adaptive Multi-Switching Chaos Synchronization of Lotka–Volterra Model to Replicate Complete and Anti-Behavior of Hindmarsh–Rose Neuron Model

Dinesh Khattar, Naokant Deo and Mukul Sirohi*

ABSTRACT: The generalized Lotka–Volterra ($\mathscr{L}$–$\mathscr{V}$) model, widely known for describing predator–prey population interactions, and the Hindmarsh–Rose ($\mathscr{H}$–$\mathscr{R}$) neuron model, a cornerstone in computational neuroscience, represent two distinct examples of nonlinear dynamical behavior in ecology and biology, respectively. In this work, an adaptive control framework is developed to achieve analytical results on multi-switching based hybrid projective synchronization between the $\mathscr{L}$–$\mathscr{V}$ and $\mathscr{H}$–$\mathscr{R}$ systems under eleven uncertain parameters. This approach relies minimally on exact parameter information, which enhances robustness and maintains efficient synchronization. Stability of synchronization errors is ensured through Lyapunov analysis. MATLAB simulations further verify the theoretical findings, demonstrating that synchronization remains successful despite the presence of multiple parameter uncertainties. Moreover, the framework encompasses several classical schemes, including complete synchronization, anti-synchronization, projective synchronization, and hybrid projective synchronization, as special cases. Alongside the synchronization results, a detailed dynamical analysis of the $\mathscr{L}$–$\mathscr{V}$ system is also conducted, providing additional insights into its complex nonlinear behavior.

Key Words: Chaos synchronization, Hindmarsh–Rose, Lotka–Volterra, multi-switching, adaptive control, Lyapunov stability.

Contents

1. Introduction

Chaos theory is a multidisciplinary field of scientific inquiry with applications in diverse domains such as mathematics, chemistry, physics, astronomy, secure communications, and management sciences [1,2,3, 4,5,6]. A deterministic system is characterized as chaotic if infinitesimal variations in its initial conditions

* Corresponding author.
2020 *Mathematics Subject Classification:* 93D05, 34D06, 34H10, 93C10.
Submitted December 12, 2025. Published February 21, 2026

lead to significantly divergent outcomes over time, a phenomenon often referred to as *sensitive dependence on initial conditions* [7]. Edward Lorenz first illustrated this concept through what is now famously known as the "butterfly effect," represented by a butterfly-shaped strange attractor in his numerical weather prediction model [8].

The study of chaotic systems typically involves the analysis of complex nonlinear differential equations, the solutions that are often analytically intractable and require computational methods for exploration. Even though chaotic behavior can emerge in low-dimensional nonlinear systems [9], the conditions for sustained chaos in smooth continuous-time autonomous systems are more restrictive. According to the Poincaré–Bendixson theorem [10], a smooth, autonomous continuous-time dynamical system governed by first-order ordinary differential equations (ODEs) cannot produce bounded chaotic trajectories when its dimension is less than three. In other words, chaotic motion in such systems requires at least three interacting state variables. Moreover, the existence of some form of nonlinear interaction in the system's equations is a necessary condition for the emergence of such complex and unpredictable behavior.

Chaos theory has progressed considerably, and one striking direction is the study of synchronization in complex dynamical systems: despite their strong sensitivity to initial conditions and apparent unpredictability, chaotic systems can be forced to synchronize using appropriate control strategies. The idea, introduced by Pecora and Carroll [11], showed that chaotic trajectories may evolve together under suitable coupling. Since then, research on chaos control and synchronization has grown both theoretically and practically, because synchronization schemes can exploit chaotic complexity to encode and transmit digital information with enhanced privacy and anonymity in communication networks [12,13,14,15]. In a typical drive–response arrangement many synchronization types appear — complete, anti-, projective, lag, and hybrid projective synchronization (HPS) among them — complete and anti-synchronization remains the most commonly studied and explored methods.

Complete synchronization occurs when the state trajectories of coupled chaotic systems evolve to coincide exactly over time, meaning that the differences between their corresponding state variables asymptotically approach zero [16,17,18]. In contrast, anti-synchronization describes the situation where the systems develop states equal in magnitude but opposite in sign, leading the sum of corresponding variables to vanish in the long run [19,20,21]. Projective synchronization extends these ideas by introducing a scaling factor, so that the response system reproduces the drive system's behavior proportionally rather than identically [22,23,24]. Hybrid synchronization broadens the concept further, allowing different synchronization behaviors—such as complete and anti-synchronization—to coexist among various state components [25,26,27]. The most generalized form, known as hybrid projective synchronization, merges the features of hybrid and projective synchronization, enabling both scaling and mixed synchronization patterns to appear simultaneously across different state variables [28,29,30]. Further theoretical elaboration on this generalization will be provided through formal remarks and mathematical analysis in Section 2.

Apart from these schemes, various synchronization strategies have also been developed over the years for identical, non-identical, chaotic, and hyperchaotic systems [31,32,33,34,35,36,37,38]. Traditional approaches primarily employ a direct, one-to-one drive–response configuration. However, many researchers have also investigated switched-based synchronization schemes [39,40,41], wherein random choices of response states are synchronized with the drives. While many existing studies employ active control strategies for their analytical simplicity, such approaches often encounter practical constraints. To address these limitations, adaptive control has been developed as a more versatile and resilient alternative, capable of achieving synchronization even when the system parameters are partially or entirely unknown [42,43,44,45]. Despite its advantages, research on synchronization schemes over chaotic and hypechaotic systems with multiple unknown parameters in the drive–response framework remains relatively limited. Unlike conventional active control, the implementation of adaptive synchronization is generally more intricate, as it requires the controller parameters to evolve as time-dependent functions rather than being selected as fixed constants. This synchronization challenge is also increased if multiple parameters are present in the drive-response equations. However, this challenge is worthwhile because it enhances the sent signal's unpredictability and ambiguity while decreasing the synchronization time, which has potential in making it a cheaper and more feasible alternative. Adaptive regulators are more resilient for another reason: they may be deployed without having prior knowledge of system parameters.

In conclusion, when such efficient controllers are integrated with multi-switched and hybrid projective strategies, they have the potential to improve the secrecy and safety of transmitted information.

This research presents the theoretical and analytical results on multi-switching based hybrid projective synchronization (MSHPS) between two n-dimensional chaotic systems. This scheme provides a large number of possible ways to synchronize two chaotic systems. We also discuss and investigate several well-known synchronization techniques, including hybrid projective synchronization (HPS), projective synchronization (PS), complete synchronization (CS), and anti-synchronization (AS), which serve as particular cases of MSHPS. To illustrate MSHPS, we consider two well-known three-dimensional deterministic models: the Generalized Lotka–Volterra model from ecology and the Hindmarsh–Rose model from biology. We first derive the analytical and theoretical basis of this synchronization for these illustrative examples. Interestingly, the synchronization process involves a total of eleven estimated system parameters, which enhances the robustness of the process. Furthermore, the synchronization outcomes are achieved through resilient and robust adaptive control, and the necessary prerequisites and conditions are established using Lyapunov stability theory. The synchronization outcomes are corroborated using MATLAB-based numerical simulations. A comparison and discussion of the novelty of this research with respect to notable published works are provided in Table 1. In addition, we explore the dynamical properties of the Generalized Lotka–Volterra model using Lyapunov exponents (LEs), time-series analysis, Poincaré cross-sections, phase portraits, and a detailed investigation of the local stability of its equilibrium points.

Table 1: Summary of recent studies on synchronization of chaotic systems.

Systems Synchronized	**System Order**	**No. of Parameters**	**Synchronization Technique**	**Control Utilized**	**References**
Identical	Integer	3	Complete	Active	[46]
Identical	Integer	3	Anti	Active	[47]
Identical	Integer	6	Complete	Adaptive	[48]
Identical	Integer and Fractional	8	Complete	Adaptive	[49]
Identical	Integer	4	Complete	Adaptive	[50]
Identical	Fractional	8	Complete	Adaptive	[51]
Identical	Integer	6	Hybrid Projective	Adaptive	[52]
Distinct	**Integer**	**11**	**Hybrid Projective with Switching**	**Adaptive**	**This work**

The organization of this manuscript is as follows: Sect. 2 discusses the generalized theory of multi-switching-based hybrid projective synchronization (MSHPS). Sect. 3 describes two three-dimensional models from ecology and biology. Sect. 4 investigates the detailed dynamical properties of the generalized Lotka–Volterra system. Sect. 5 provides an illustrative example with a rigorous analytical proof, based on Lyapunov theory, to demonstrate HPS via robust adaptive control between two distinct models. In Sects. 6 and 7, two specific scenarios of the hybrid projective method are examined and compared through numerical simulation. Finally, Sect. 8 concludes the manuscript by summarizing the main findings, highlighting the novelties, and outlining potential directions for future research.

2. Problem Formulation

This section presents analytical results on the synchronization of two chaotic systems in n dimensions using a multi-switching–based hybrid projective synchronization (MSHPS) scheme.

Suppose a drive model is given by

$$\dot{\psi}(t) = H(\psi), \tag{2.1}$$

where the drive variables are expressed as $\psi(t) = (\psi_1(t), \psi_2(t), \ldots, \psi_n(t))^\top \in \mathbb{R}^n$, and $H : \mathbb{R}^n \to \mathbb{R}^n$ is a smooth nonlinear function.

Assume an associated response model:

$$\dot{\zeta}(t) = J(\zeta) + \Omega(\psi, \zeta), \tag{2.2}$$

where the response variables are given by $\zeta(t) = (\zeta_1(t), \zeta_2(t), \ldots, \zeta_n(t))^\top \in \mathbb{R}^n$, and $J : \mathbb{R}^n \to \mathbb{R}^n$ is also a smooth nonlinear function. The term $\Omega(\psi, \zeta)$ denotes the adaptive-based control.

Definition 2.1 *The response model in (2.2) achieves* generalized hybrid-projective synchronization *with the drive model in (2.1) if*

$$\lim_{t\to\infty} \| \underbrace{\mathcal{B}\zeta(t) - \mathcal{A}\psi(t)}_{e(t)} \| = 0,$$

where $\mathcal{B} = \text{diag}(\beta_1, \beta_2, \beta_3, \ldots, \beta_n)$, $\mathcal{A} = \text{diag}(\delta_1, \delta_2, \delta_3, \ldots, \delta_n)$ *are arbitrary but nonzero diagonal matrices in* $\mathbb{R}^{n\times n}$, *and* $e(t)$ *represents the synchronization error.*

Component-wise, this is equivalent to:

$$\lim_{t\to\infty} \|e_k(t)\| = \lim_{t\to\infty} \|\beta_k\zeta_k(t) - \delta_l\psi_l(t)\| = 0,$$

where $e(t) = [e_1(t), e_2(t), \ldots, e_n(t)]^\top$, *and* $k, l \in \{1, 2, \ldots, n\}$.

Remark 2.1 *Each component* $e_k(t)$ *can be rewritten as:*

$$e_{k_{(kl)}}(t) = \beta_k\zeta_k(t) - \delta_l\psi_l(t),$$

where $e(t) = \left(e_{1_{(kl)}}, e_{2_{(kl)}}, \ldots, e_{n_{(kl)}}\right)^\top$. *Here, the subscript* (kl) *indicates that the* k*-th component corresponds to the* k*-th element of* $\mathcal{B}\zeta(t)$ *and the* l*-th component corresponds to* l*-th element of* $\mathcal{A}\psi(t)$.

Remark 2.2 *In Definition 2.1, the error components* $e_{k_{(kl)}}$ *are indexed with two indices* (k, l), *which can be chosen in two ways: either with* $k = l$ *or with* $k \neq l$. *These indexing choices correspond to different synchronization configurations.*

Specifically, the components for a 3D system can be grouped as:

$$\begin{cases} \text{If } k = l: & e_{1_{(11)}}, \quad e_{2_{(22)}}, \quad e_{3_{(33)}}. & \text{(Traditional synchronization)} \\ \text{If } k \neq l: & e_{1_{(12)}}, \quad e_{1_{(13)}}, \quad e_{2_{(21)}}, \quad e_{2_{(23)}}, \quad e_{3_{(31)}}, \quad e_{3_{(32)}}. & \text{(Switched synchronization)} \end{cases}$$

In a more generalized form, the case $k = l$ *leads to conventional synchronization schemes, while* $k \neq l$ *enables multi-switching hybrid projective synchronization (MSHPS), producing a broader variety of error dynamics between the drive and response systems. This switching mechanism introduces a large set of possible error combinations, which significantly enhances the cryptographic complexity of the transmitted signal. From a secure communication perspective, it becomes much harder for an intruder to predict the actual synchronization pattern. When integrated with adaptive control, this approach offers even greater robustness and resistance against potential attacks.*

Definition 2.2 *Based on Definition 2.1, if the matrix* $\mathcal{B}$ *is chosen as the identity matrix* $I_{n\times n}$, *then the response model attains* hybrid projective synchronization (HPS) *with the drive model if*

$$\lim_{t\to\infty} \| \underbrace{\zeta(t) - \mathcal{A}\psi(t)}_{e(t)} \| = 0.$$

Remark 2.3 *The HPS scheme reduces to the conventional* projective synchronization (PS) *problem if the matrix* $\mathcal{A} = \text{diag}(\delta_1, \delta_2, \ldots, \delta_n)$ *is specified such that* $\delta_i = \delta \neq 0$ *for all* $i = 1, 2, \ldots, n$.

Remark 2.4 *The PS framework further simplifies to the* hybrid synchronization (HS) *case if the diagonal entries of* $\mathcal{A}$ *are alternatively selected as* $\delta_i = \pm 1$.

Remark 2.5 *The PS problem reduces to the well-known* identical synchronization (IS) *or* complete synchronization (CS) *case when* $\mathcal{A} = I_{n\times n}$.

Remark 2.6 *Similarly, PS transforms into the* anti-synchronization (AS) *scheme when* $\mathcal{A} = -I_{n\times n}$.

3. Systems Description

3.1. Hindmarsh–Rose ($\mathscr{H}$–$\mathscr{R}$) neuron model

The three-dimensional continuous-time Hindmarsh–Rose ($\mathscr{H}$–$\mathscr{R}$) model is a widely used neuronal model that describes the membrane potential dynamics of an individual neuron [53]. It captures both spiking and bursting neuronal behaviors through nonlinear interactions across multiple time scales. The $\mathscr{H}$–$\mathscr{R}$ model is defined by the system:

$$\begin{cases} \dfrac{dx}{dt} = \phi(x) + y - z + I, \\ \dfrac{dy}{dt} = \psi(x) - y, \\ \dfrac{dz}{dt} = r\big[k(x - x_0) - z\big], \end{cases} \tag{3.1}$$

where the membrane potential x, recovery variable y, and slow adaptation current z evolve over time. The nonlinear functions $\phi(x) = bx^2 - ax^3$ and $\psi(x) = c - dx^2$ represent the intrinsic ionic currents influencing the membrane potential and recovery processes, respectively. The parameter $r > 0$ controls the slow time-scale dynamics of the variable z while I denotes the external current input which can be constant or time-varying. The parameters a, b, c, d, k and x_0 govern the overall dynamics and neuronal firing patterns.

3.2. Generalized Lotka–Volterra ($\mathscr{L}$–$\mathscr{V}$) model

The generalized Lotka–Volterra ($\mathscr{L}$–$\mathscr{V}$) model [54] provides a classical framework for investigating complex ecological interactions. It is expressed as a 3D system of nonlinear differential equations:

$$\begin{cases} \dfrac{dw}{dt} = pw^2 + w - ws - muw^2, \\ \dfrac{ds}{dt} = ws - s, \\ \dfrac{du}{dt} = muw^2 - nu, \end{cases} \tag{3.2}$$

where $w(t)$ represents the prey population, $s(t)$ the predator population, and $u(t)$ an additional ecological variable, such as a resource or a competing species. The positive constants p, m, and n define the intrinsic growth rates and interaction strengths.

4. Dynamical Insights of the $\mathscr{L}$–$\mathscr{V}$ Model

4.1. Lyapunov exponents

Lyapunov exponents (LEs) describe how nearby trajectories in a dynamical system separate or come together on average, thus providing a quantitative way to assess sensitivity to initial conditions. When at least one exponent is positive, the system exhibits chaotic motion; a zero value usually corresponds to periodic or quasi-periodic behavior, while negative exponents indicate dissipative tendencies that cause trajectories to settle toward attractors. In the present work, the Wolf algorithm [55] is used to calculate the Lyapunov spectrum of the $\mathscr{L}$–$\mathscr{V}$ model. The system started from the initial condition $(w_0, s_0, u_0) = (1.01, 1.01, 1.01)$, with parameters $(p, n, m) = (30, 3, 2.7)$, and is numerically integrated using a step size of $\Delta t = 0.5$. The resulting Lyapunov exponents are $LE_1 = 0.0283$, $LE_2 = 0.0001 \approx 0$, and $LE_3 = -0.0293$, computed over a sufficiently long interval of $t = 10000$. The full spectrum is shown in Fig. 1. Although the sum of the exponents is close to zero, implying near-conservative behavior, the presence of a positive maximum exponent indicates that the system evolves with mild-chaos. However, further analysis is required to confirm the presence of a strong chaotic behavior.

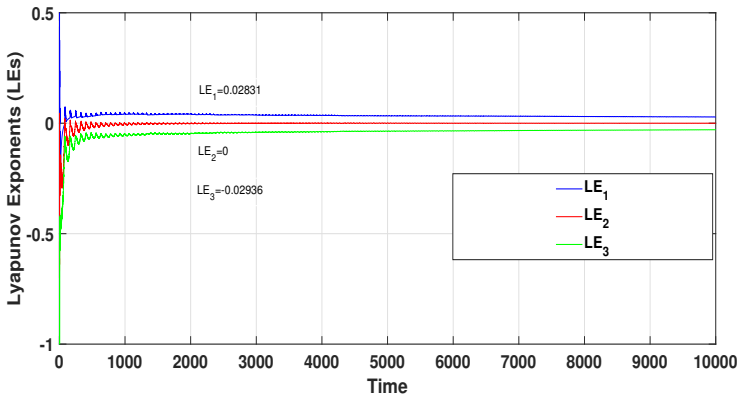

Figure 1: Lyapunov spectrum for the $\mathscr{L}$–$\mathscr{V}$ model.

4.2. Phase portraits

In chaotic systems, trajectories that start from nearby initial conditions tend to diverge exponentially over time, yet their nonlinear folding mechanism is confined within a bounded regions of the phase space, giving rise to distinctive attractors. Phase portraits represents these trajectories, revealing how the system evolves over time and shedding light on its underlying dynamical behavior.

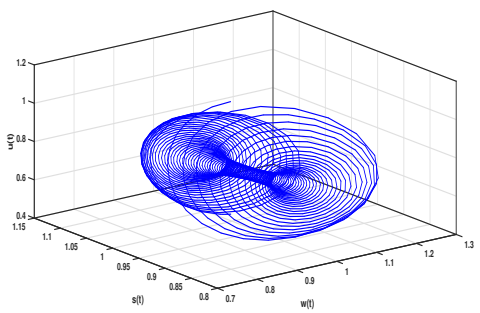

Figure 2: Phase portrait of the $\mathscr{L}$–$\mathscr{V}$ model with parameters $(p, m, n) = (2, 2.9851, 3)$.

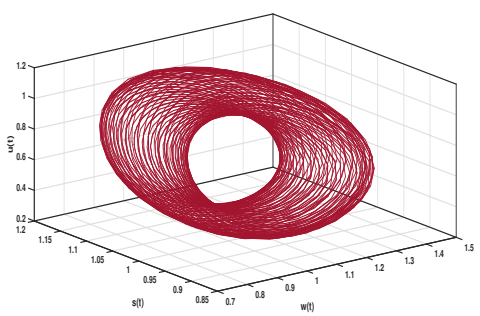

Figure 3: Phase portrait of the $\mathscr{L}$–$\mathscr{V}$ model with parameters $(p, m, n) = (2, 2.895, 3)$.

Figures 2 and 3 illustrate the phase portraits of the $\mathscr{L}$–$\mathscr{V}$ model for two different parameter sets, showcasing distinct dynamical regimes.

4.3. Time series

A time series is a collection of data points observed at successive and usually equally spaced time intervals. Analyzing such data helps reveal the underlying dynamics of a system and can also aid in forecasting its future behavior. In dynamical systems, the evolution of state variables over time offers valuable clues about the system's character: irregular or unpredictable fluctuations suggest chaotic behavior, while regular oscillations indicate periodic or quasi-periodic motion. The time evolution of the variables in the $\mathscr{L}$–$\mathscr{V}$ model is illustrated in Fig. 4.

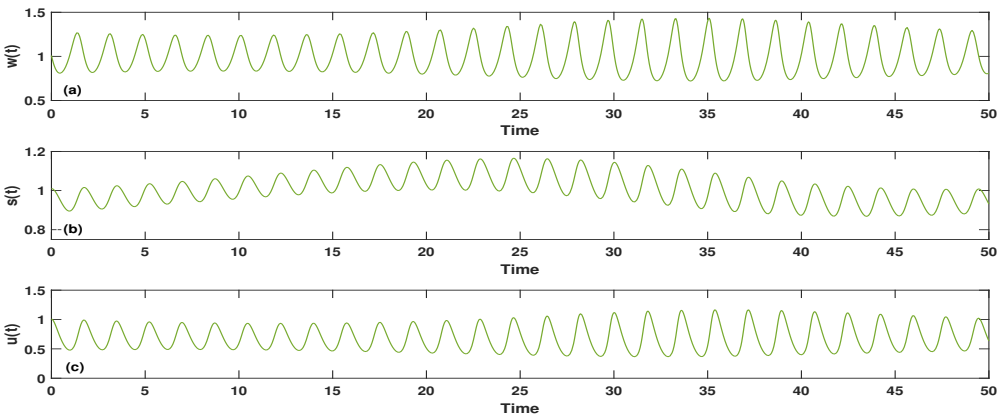

Figure 4: Time series for the $\mathscr{L}$–$\mathscr{V}$ model: **(a)** $w(t)$, **(b)** $s(t)$, and **(c)** $u(t)$ versus time.

4.4. Poincaré section

A Poincaré section is a renowned technique that is used to simplify the analysis of deterministic dynamical models by observing the points at which trajectories intersect a selected lower-dimensional surface. Recording these successive intersection points yields a discrete representation of the system, known as the Poincaré map, which preserves the essential features of the system's dynamics. This approach is particularly useful for distinguishing between the periodic, quasi-periodic, and chaotic nature of the system, as it provides a compact visualization of the system's complex trajectories. The Poincaré sections of the $\mathscr{L}$–$\mathscr{V}$ model, projected onto the w–s and w–u planes, are illustrated in Fig. 5.

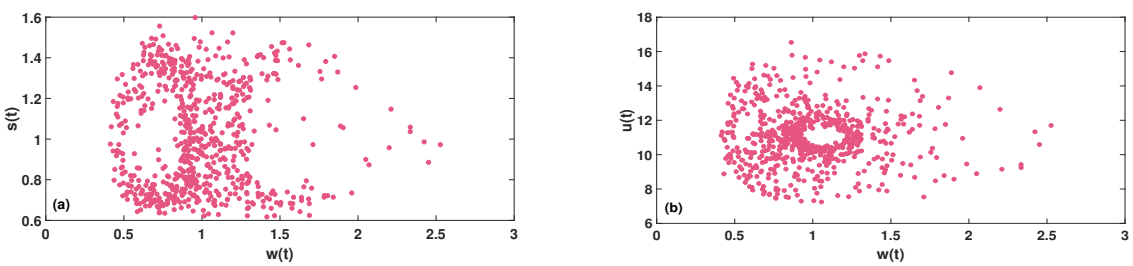

Figure 5: Poincaré map of the $\mathscr{L}$–$\mathscr{V}$ model: **(a)** projection onto the w-s plane, and **(b)** projection onto the w-u plane.

4.5. Stability analysis

Equilibrium points in deterministic dynamical systems are points in the phase space where the system remains constant over time, meaning the rates of change are zero. At these points, there is no net evolution in the system's behavior.

To find the equilibrium points of the $\mathscr{L}$–$\mathscr{V}$ model, we solve the following system:

$$\begin{cases} w - ws + 30w^2 - 2.7uw^2 = 0, \\ ws - s = 0, \\ 2.7uw^2 - 3u = 0. \end{cases}$$

Using MATLAB, we obtain three equilibrium points:

$$E_1 = (0,0,0)^\top, \quad E_2 = (-0.0333,0,0)^\top, \quad E_3 = (1,8.3783,0)^\top.$$

The Jacobian matrix J of the system is given by

$$J = \begin{bmatrix} 1 - s + 60w - 5.4uw & -w & -2.7w^2 \\ s & w - 1 & 0 \\ 5.4uw & 0 & 2.7w^2 - 3 \end{bmatrix}.$$

According to the Hartman–Grobman theorem [56], the stability of these equilibrium points can be determined by analyzing the eigenvalues of J evaluated at each point. The eigenvalues are:

$$\begin{cases} \text{At } E_1: & \gamma_{11} = -3.0000, & \gamma_{12} = -1.0000, & \gamma_{13} = 1.0000, \\ \text{At } E_2: & \gamma_{21} = -0.9980, & \gamma_{22} = -1.0333, & \gamma_{23} = -2.9970, \\ \text{At } E_3: & \gamma_{31} = 52.4620, & \gamma_{32} = 0.1597, & \gamma_{33} = -0.3000. \end{cases}$$

Since the equilibrium point E_1 has an eigenvalue with a positive real part ($\gamma_{13} = 1$), it is locally unstable. Similarly, E_3 is also locally unstable due to two eigenvalues with positive real parts (γ_{31} and γ_{32}). In contrast, all eigenvalues at E_2 have negative real parts, indicating that E_2 is asymptotically locally stable. Therefore, the predator-prey model has one local stable and two locally unstable equilibrium points. The dynamics of the $\mathscr{L}$–$\mathscr{V}$ model evolve around these points in phase space.

5. Illustrative Example of Synchronization

Although the analytical proofs shown here corresponds to the conventional HPS configuration ($k = l$), the proposed Lyapunov-based adaptive control design and error structure are general and valid for multi-switching configurations ($k \neq l$). In principle, the same convergence proof guarantees that the synchronization errors approach zero asymptotically under any admissible switching of the error components, thereby validating the proposed multi-switching based hybrid projective synchronization (MSHPS) framework. Thus, we present a theoretical implementation of synchronization for ($k = l$) framework discussed earlier in Sec. 2. Synchronization will be achieved via a rigorous yet efficient adaptive control approach.

We select the $\mathscr{H}$–$\mathscr{R}$ model as the drive system, defined by

$$\begin{cases} \dot{x} = y - ax^3 + bx^2 - z + I, \\ \dot{y} = c - dx^2 - y, \\ \dot{z} = Rx - J - rz, \end{cases} \tag{5.1}$$

where the parameters satisfy $R = rk$ and $J = rkx_0$.

The $\mathscr{L}$–$\mathscr{V}$ model is chosen as the response system, described by

$$\begin{cases} \dot{w} = w - ws + pw^2 - muw^2 + \Omega_1(t), \\ \dot{s} = ws - s + \Omega_2(t), \\ \dot{u} = muw^2 - nu + \Omega_3(t), \end{cases} \tag{5.2}$$

where $\Omega_1(t), \Omega_2(t)$, and $\Omega_3(t)$ are the control functions to be designed to achieve HPS between the $\mathscr{H}$–$\mathscr{R}$ and $\mathscr{L}$–$\mathscr{V}$ models using an adaptive control strategy.

For achieving traditional or multi-switching-based synchronization, multiple configurations are possible depending on whether $k = l$ or $k \neq l$. For theoretical analysis, we adopt the conventional choice $k = l$,

whereby the synchronization errors are defined as the difference between the response and drive systems with an intervening scaling factor. Specifically, from Remark 2.2, we define the individual synchronization errors as $e_{1_{(11)}}, e_{2_{(22)}}$, and $e_{3_{(33)}}$. For notational simplicity, we represent theses synchronization error vector in the compact form

$$\mathbf{e}(t) = \begin{pmatrix} e_{1_{(11)}} \\ e_{2_{(22)}} \\ e_{3_{(33)}} \end{pmatrix} = \begin{pmatrix} e_1 \\ e_2 \\ e_3 \end{pmatrix} = \begin{pmatrix} w - \delta_1 x \\ s - \delta_2 y \\ u - \delta_3 z \end{pmatrix}, \tag{5.3}$$

where each $\delta_i \neq 0$ is a scaling parameter.

Taking the time derivative, the error dynamics become

$$\begin{cases} \dot{e}_1 = \dot{w} - \delta_1 \dot{x}, \\ \dot{e}_2 = \dot{s} - \delta_2 \dot{y}, \\ \dot{e}_3 = \dot{u} - \delta_3 \dot{z}. \end{cases} \tag{5.4}$$

Substituting the dynamics from (5.1) and (5.2) into (5.4), we get

$$\begin{cases} \dot{e}_1 = w - ws + pw^2 - muw^2 - \delta_1 \left(y - ax^3 + bx^2 - z + I\right) + \Omega_1(t), \\ \dot{e}_2 = ws - s - \delta_2 \left(c - dx^2 - y\right) + \Omega_2(t), \\ \dot{e}_3 = muw^2 - nu - \delta_3 \left(Rx - J - rz\right) + \Omega_3(t). \end{cases} \tag{5.5}$$

It is essential to construct the adaptive control inputs $\Omega(t) = [\Omega_1(t), \Omega_2(t), \Omega_3(t)]^\top$ and an associated parameter update law such that the synchronization error $e(t)$ converges to zero. These controls and adaptation laws must satisfy Lyapunov stability criteria to guarantee asymptotic stability of the error dynamics in (5.5). The following theorem establishes these results.

Theorem 5.1 *The $\mathscr{L}$–$\mathscr{V}$ and $\mathscr{H}$–$\mathscr{R}$ models attain asymptotic hybrid projective synchronization (HPS) for an assigned scaling matrix $\delta = \mathrm{diag}(\delta_1, \delta_2, \delta_3)$, and the parameters $p, m, a, b, I, c, d, R, J, n, r$ can be simultaneously estimated by choosing the adaptive control vector $\Omega(t) = [\Omega_1(t), \Omega_2(t), \Omega_3(t)]^\top$ as*

$$\begin{cases} \Omega_1(t) = & ws - w - \hat{P}(t)w^2 + \hat{M}(t)uw^2 + \delta_1 y - \delta_1 \hat{A}(t)x^3 + \delta_1 \hat{B}(t)x^2 \\ & -\delta_1 z + \delta_1 \hat{I}(t) - K_1 e_1, \\ \Omega_2(t) = & s - ws + \delta_2 \hat{C}(t) - \delta_2 \hat{D}(t)x^2 - \delta_2 y - K_2 e_2, \\ \Omega_3(t) = & \hat{N}(t)u - \hat{M}(t)uw^2 + \delta_3 \hat{R}(t)x - \delta_3 \hat{J}(t) - \delta_3 \hat{r}(t)z - K_3 e_3. \end{cases} \tag{5.6}$$

Furthermore, the parameter update laws are given by

$$\begin{cases} \dot{\hat{P}}(t) & = e_1 w^2 - K_4 e_p, \\ \dot{\hat{M}}(t) & = e_3 uw^2 - e_1 uw^2 - K_5 e_m, \\ \dot{\hat{A}}(t) & = \delta_1 e_1 x^3 - K_6 e_a, \\ \dot{\hat{B}}(t) & = -\delta_1 e_1 x^2 - K_7 e_b, \\ \dot{\hat{I}}(t) & = -e_1 - K_8 e_I, \\ \dot{\hat{C}}(t) & = -\delta_2 e_2 - K_9 e_c, \\ \dot{\hat{D}}(t) & = \delta_2 e_2 x^2 - K_{10} e_d, \\ \dot{\hat{R}}(t) & = -\delta_3 e_3 x - K_{11} e_R, \\ \dot{\hat{J}}(t) & = \delta_3 e_3 - K_{12} e_J, \\ \dot{\hat{N}}(t) & = -e_3 u - K_{13} e_n, \\ \dot{\hat{r}}(t) & = \delta_3 e_3 z - K_{14} e_r, \end{cases} \tag{5.7}$$

where the estimated parameter errors are defined as
$e_p = \hat{P}(t) - p$, $e_m = \hat{M}(t) - m$, $e_a = \hat{A}(t) - a$, $e_b = \hat{B}(t) - b$, $e_I = \hat{I}(t) - I, e_c = \hat{C}(t) - c$, $e_d = \hat{D}(t) - d$, $e_R = \hat{R}(t) - R$, $e_J = \hat{J}(t) - J$, $e_n = \hat{N}(t) - n$, $e_r = \hat{r}(t) - r$, *all control and parametric-gains satisfy* $K_\varrho > 0$ *for* $\varrho = 1, 2, \ldots, 14$.

Proof: Consider the Lyapunov function

$$V(t) = \frac{1}{2}\Big(e_1^2 + e_2^2 + e_3^2 + e_p^2 + e_m^2 + e_a^2 + e_b^2 + e_I^2 + e_c^2 + e_d^2 + e_R^2 + e_J^2 + e_n^2 + e_r^2\Big),$$

which is positive definite. Taking the time derivative yields

$$\begin{aligned}\dot{V}(t) = {} & e_1\dot{e}_1 + e_2\dot{e}_2 + e_3\dot{e}_3 + e_p\dot{e}_p + e_m\dot{e}_m + e_a\dot{e}_a + e_b\dot{e}_b + e_I\dot{e}_I + e_c\dot{e}_c + e_d\dot{e}_d \\ & + e_R\dot{e}_R + e_J\dot{e}_J + e_n\dot{e}_n + e_r\dot{e}_r. \end{aligned} \tag{5.8}$$

Substituting the error dynamics (5.5) and control laws (5.6) along with parameter update rules (5.7) into (5.8), after simplification we get

$$\begin{aligned}\dot{V}(t) &= -K_1e_1^2 - K_2e_2^2 - K_3e_3^2 - K_4e_p^2 - K_5e_m^2 - K_6e_a^2 - K_7e_b^2 - K_8e_I^2 \\ &\quad - K_9e_c^2 - K_{10}e_d^2 - K_{11}e_R^2 - K_{12}e_J^2 - K_{13}e_n^2 - K_{14}e_r^2 \\ &= -e^TKe < 0,\end{aligned}$$

where $K = \begin{pmatrix} K_1 & 0 & 0 & \cdots & 0 \\ 0 & K_2 & 0 & \cdots & 0 \\ 0 & 0 & K_3 & \cdots & 0 \\ \vdots & \vdots & \vdots & \ddots & \vdots \\ 0 & 0 & 0 & \cdots & K_{14} \end{pmatrix}$ and $e = [\, e_1, e_2, e_3, e_p, e_m, e_a, e_b, e_I, e_c, e_d, e_R, e_J, e_n, e_r \,]^\top$

By Barbalat's lemma [57], since $\dot{V}(t)$ is negative definite, it follows that

$$\lim_{t\to\infty} \|e(t)\| = 0.$$

Thus, the synchronization errors and parameter estimation errors converge to zero asymptotically, proving that the $\mathscr{L}$–$\mathscr{V}$ and $\mathscr{H}$–$\mathscr{R}$ models achieve asymptotic hybrid projective synchronization ($k = l$) via adaptive control scheme under eleven parametric uncertainties. ■ □

6. Numerical Simulations

In this section, we present numerical simulations based on the analytical proofs of hybrid projective synchronization derived in the preceding section. This approach provides an effective means to verify and validate the theoretical results obtained from the chaotic synchronization methodology. The simulations are carried out on the MATLAB platform. The parameter values chosen for the $\mathscr{L}$–$\mathscr{V}$ and $\mathscr{H}$–$\mathscr{R}$ systems in each computation are: $a = 1, b = 3, c = 1, d = 5, J = 0.032, I = 3.25, r = 0.005, R = 0.02, m = 2.7, n = 3$, and $p = 30$. The initial conditions for the drive ($\mathscr{H}$–$\mathscr{R}$) 3D model are $x(0) = 1$, $y(0) = 2$, $z(0) = 1$, while those for the response ($\mathscr{L}$–$\mathscr{V}$) 3D model are $w(0) = 6$, $s(0) = 4$, $u(0) = 3$. These values are selected to ensure that both models exhibit complex patterns in the absence of any controller $\Omega(t)$. Although the numerical demonstration shown here corresponds to the conventional HPS configuration ($k = l$), the proposed Lyapunov-based adaptive control design and error structure are general and valid for multi-switching configurations ($k \neq l$). In principle, the same convergence proof guarantees that the synchronization errors approach zero asymptotically under any admissible switching of the error components, thereby validating the proposed multi-switching based hybrid projective synchronization (MSHPS) framework.

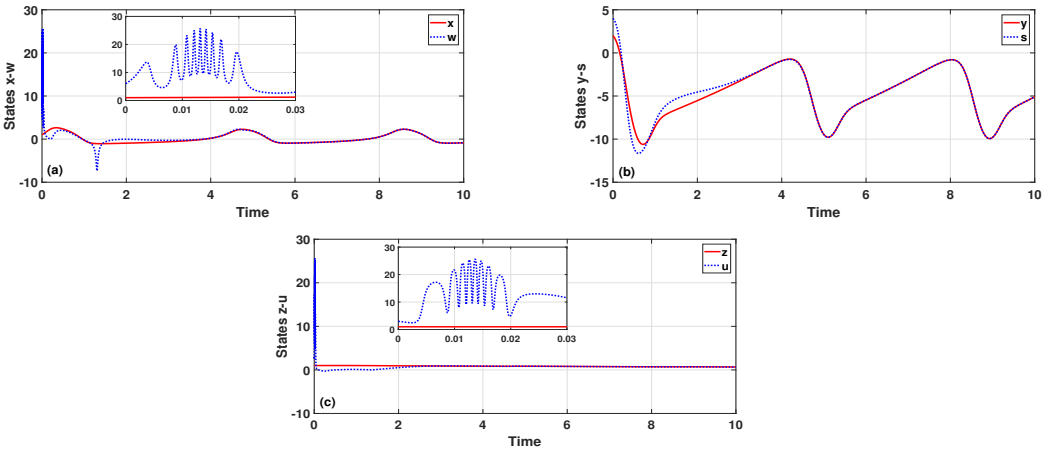

Figure 6: Time evolution of the states of the $\mathscr{L}$–$\mathscr{V}$ and $\mathscr{H}$–$\mathscr{R}$ models under complete synchronization: **(a)** x and w, **(b)** y and s, and **(c)** z and u.

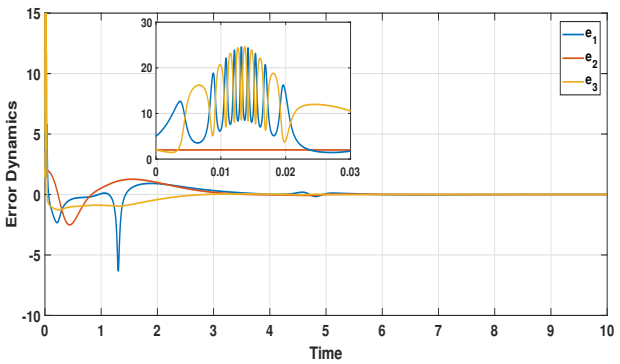

Figure 7: Temporal profiles of the e_1, e_2, and e_3 during complete-synchronization.

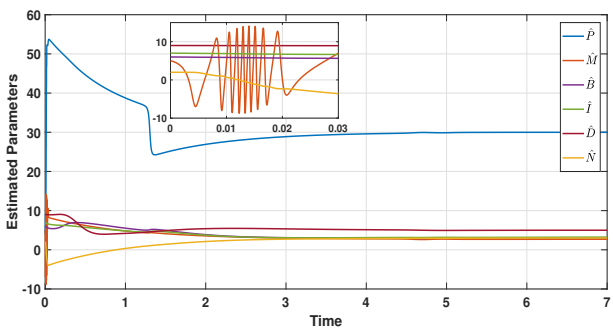

Figure 8: Evolution of the estimated parameters $\hat{P}, \hat{M}, \hat{B}, \hat{I}, \hat{D}$, and $\hat{N}$ during complete-synchronization.

7. Comparative Analysis

We compare two particular cases of hybrid projective technique, namely anti-synchronization and complete synchronization. Since adaptive controllers are employed, the convergence of the estimated parameters is observed alongside the asymptotic convergence of synchronization errors, i.e., $e = (e_1, e_2, e_3)^\top$

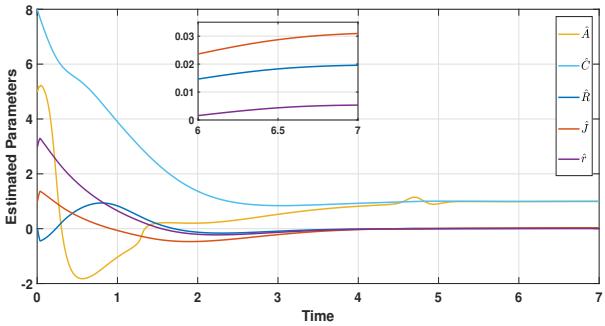

Figure 9: Evolution of the estimated parameters $\hat{A}, \hat{C}, \hat{R}, \hat{J}$, and $\hat{r}$ during complete synchronization.

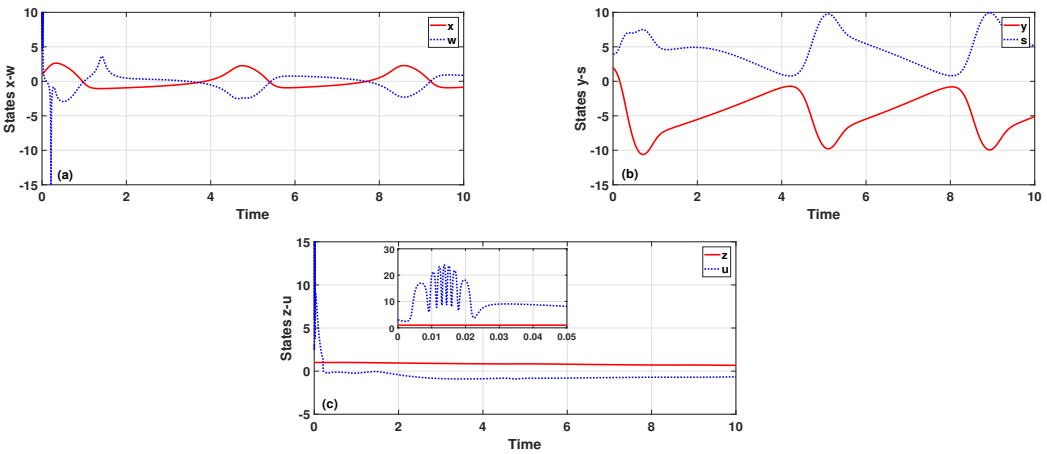

Figure 10: Time evolution of the states of the $\mathscr{L}$-$\mathscr{V}$ and $\mathscr{H}$-$\mathscr{R}$ models under anti-synchronization: **(a)** x and w, **(b)** y and s, and **(c)** z and u.

$\longrightarrow \mathbf{0}$. We first consider the case of complete synchronization, which corresponds to uniformly setting the scaling factors as $\delta_\varrho = 1$ for all ϱ. The numerical simulation results for the time evolution of the state variables of the $\mathscr{L}$–$\mathscr{V}$ and $\mathscr{H}$–$\mathscr{R}$ systems, when the adaptive controller $\Omega(t)$ is applied to the response system ($\mathscr{L}$–$\mathscr{V}$) in the case of complete synchronization, are presented in Fig. 6. The temporal profiles of the complete synchronization error dynamics are shown in Fig. 7, where the control and parametric gains are set to $K_\varrho = 5$ for $\varrho = 1, 2, 3, \ldots, 14$. It is noteworthy that as $t \to \infty$, the synchronization error e converges asymptotically to zero, confirming that the states achieve complete synchronization. Moreover, in our case, due to the adaptive control law, the estimated parameters converge to their actual values, i.e.,$\hat{A} \longrightarrow a, \hat{B} \longrightarrow b, \hat{C} \longrightarrow c, \hat{D} \longrightarrow d, \hat{J} \longrightarrow J, \hat{I} \longrightarrow I, \hat{r} \longrightarrow r, \hat{R} \longrightarrow R, \hat{M} \longrightarrow m, \hat{N} \longrightarrow n, \hat{P} \longrightarrow p$, as illustrated in Fig. 8 and Fig. 9. It is important to note that this parametric convergence to its true value is not always guaranteed and depends on several factors.

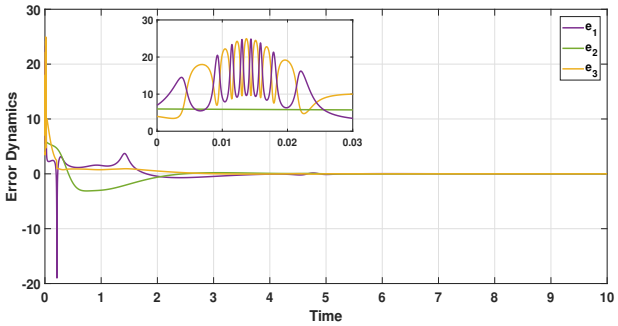

Figure 11: Temporal profiles of the e_1, e_2, and e_3 during anti-synchronization.

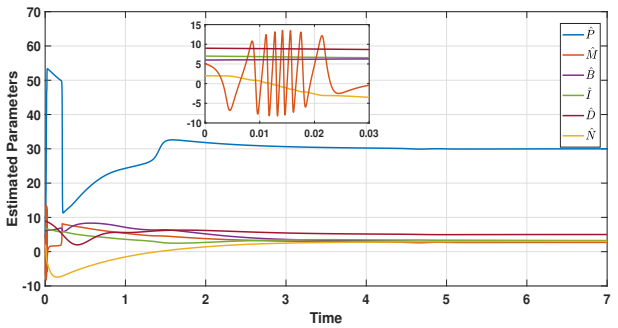

Figure 12: Evolution of the estimated parameters $\hat{P}, \hat{M}, \hat{B}, \hat{I}, \hat{D}$, and $\hat{N}$ during anti-synchronization.

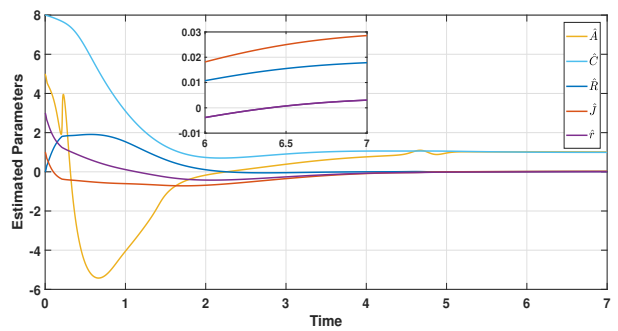

Figure 13: Evolution of the estimated parameters $\hat{A}, \hat{C}, \hat{R}, \hat{J}$, and $\hat{r}$ during anti-synchronization.

Similarly, when we consider the case of anti-synchronization, which corresponds to uniformly setting the scaling factors as $\delta_\varrho = -1$ for all ϱ. The numerical simulation results for the time evolution of the state variables of the $\mathscr{L}$–$\mathscr{V}$ and $\mathscr{H}$–$\mathscr{R}$ systems, when the adaptive controller $\Omega(t)$ is applied to the response system ($\mathscr{L}$–$\mathscr{V}$) in case of anti-synchronization, are presented in Fig. 10. The temporal profiles of the anti-synchronization error dynamics are shown in Fig. 11, where the control and parametric gains are set to $K_\varrho = 5$ for $\varrho = 1, 2, 3, \ldots, 14$. It is noteworthy that as $t \to \infty$, the anti-synchronization error e converges asymptotically to zero, confirming that the states achieve anti-synchronization. Moreover, in our case, due to the adaptive control law, the estimated parameters converge to their actual values, i.e., $\hat{A} \longrightarrow a, \hat{B} \longrightarrow b, \hat{C} \longrightarrow c, \hat{D} \longrightarrow d, \hat{J} \longrightarrow J, \hat{I} \longrightarrow I, \hat{r} \longrightarrow r, \hat{R} \longrightarrow R, \hat{M} \longrightarrow m, \hat{N} \longrightarrow n, \hat{P} \longrightarrow p$, as illustrated in Fig. 12 and Fig. 13.

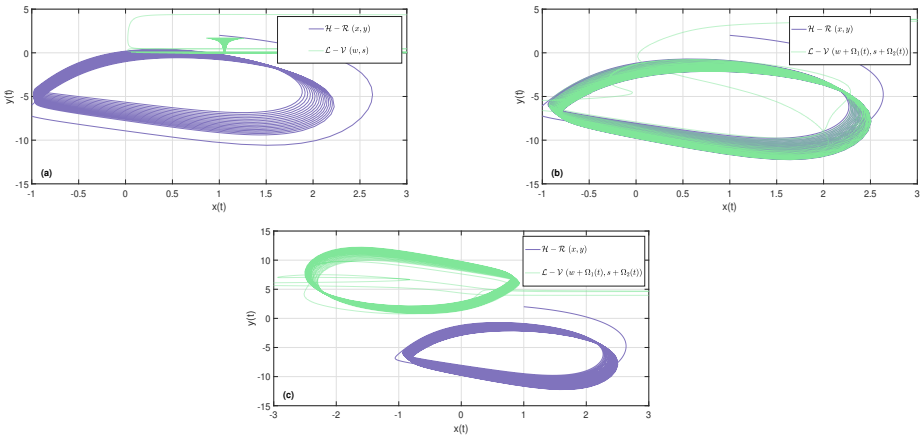

Figure 14: The dynamics of the $\mathscr{H}$–$\mathscr{R}$ and $\mathscr{L}$–$\mathscr{V}$ models in the x–y plane: (a) unsynchronized behavior, (b) adaptive-control-based complete synchronization, and (c) adaptive-control-based anti-synchronization.

Furthermore, the unsynchronized behavior and the adaptive synchronization of the Lotka–Volterra model replicating the complete and anti-synchronization behaviors of the Hindmarsh–Rose neuron model in the x–y plane can be observed in Figure 14.

8. Conclusion

In this work, we studied a multi-switching hybrid projective synchronization (MSHPS) framework for synchronizing two distinct deterministic models that represent paradigms of nonlinear dynamics in ecology and biology. Theoretical guarantees were established using Lyapunov stability theory, while adaptive control ensured robustness against parameter uncertainties, enabling synchronization without requiring precise knowledge of system parameters. Extensive MATLAB-based simulations are used to validate the analytical theory, demonstrating that both complete and anti-synchronization are effectively achieved. Furthermore, the synchronization errors asymptotically approach zero, and the adaptive parametric estimates converge to their actual values under the particular system parameters and initial conditions. These results confirm the theoretical framework, emphasize the robustness and flexibility of the proposed control approach. Moreover, conventional synchronization schemes—such as complete, projective, hybrid, and anti-synchronization—emerge as special cases of the studied MSHPS methodology. In summary, the proposed framework presents a consistent and reliable synchronization strategy, grounded in rigorous theoretical analysis and supported by numerical validation, offering a unified perspective that may inspire future work in ecological modeling, biological systems, and secure communication networks. In addition to synchronization analysis, the intrinsic dynamics of the generalized Lotka–Volterra system is also investigated. The Lyapunov spectrum revealed weakly dissipative, near-conservative characteristics, while the corresponding phase portraits for specific parameter settings exhibited annular and torus-like attractors, underscoring the system's rich dynamical behavior.

Acknowledgments

The authors would like to thank the anonymous reviewers for their valuable feedback and suggestions, which significantly improved the quality of this manuscript. The corresponding author, Mukul Sirohi, would also like to express his gratitude to Delhi Technological University, Delhi, India, for its support.

References

1. R. Devaney, An introduction to chaotic dynamical systems, CRC Press, New York, (2018).

2. I. R. Epstein, Oscillations and chaos in chemical systems, Physica D: Nonlinear Phenom. 7(1–3), 47–56, (1983). https://doi.org/10.1016/0167-2789(83)90114-8

3. N. Gisin, Indeterminism in physics, classical chaos and Bohmian mechanics: are real numbers really real?, Erkenntnis 86(6), 1469–1481, (2021). https://doi.org/10.1007/s10670-019-00165-8

4. A. A. Trani, N. W. Leigh, T. C. Boekholt, S. P. Zwart, Isles of regularity in a sea of chaos amid the gravitational three-body problem, Astron. Astrophys. 689, A24, (2024). https://doi.org/10.1051/0004-6361/202449862

5. W. Cao, H. Cai, Z. Hua, n-Dimensional chaotic map with application in secure communication, Chaos Solitons Fractals 163, 112519, (2022). https://doi.org/10.1016/j.chaos.2022.112519

6. P. Murphy, Chaos theory as a model for managing issues and crises, Public Relat. Rev. 22(2), 95–113, (1996). https://doi.org/10.1016/S0363-8111(96)90001-6

7. S. H. Strogatz, Nonlinear dynamics and chaos: with applications to physics, biology, chemistry, and engineering, Chapman and Hall/CRC, New York, (2024).

8. E. N. Lorenz, Deterministic nonperiodic flow, J. Atmos. Sci. 20(2), 130–141, (1963). https://doi.org/10.1175/1520-0469(1963)020¡0130:DNF¿2.0.CO;2

9. Z. A. Rahman, B. H. Jasim, Y. I. Al-Yasir, Chaotic dynamics in the 2D system of nonsmooth ordinary differential equations, Iraqi J. Comput. Sci. Math. 3(2), 2, (2022). https://doi.org/10.52866/ijcsm.2022.02.01.002

10. M. W. Hirsch, R. L. Devaney, S. Smale, Differential equations, dynamical systems, and linear algebra, Academic Press, New York, (1974).

11. L. M. Pecora, T. L. Carroll, Synchronization in chaotic systems, Phys. Rev. Lett. 64(8), 821–824, (1990). https://doi.org/10.1103/PhysRevLett.64.821

12. W. Kinzel, A. Englert, I. Kanter, On chaos synchronization and secure communication, Philos. Trans. R. Soc. A 368(1911), 379–389, (2010). https://doi.org/10.1098/rsta.2009.0230

13. W. Shao, Y. Fu, M. Cheng, L. Deng, D. Liu, Chaos synchronization based on hybrid entropy sources and applications to secure communication, IEEE Photonics Technol. Lett. 33(18), 1038–1041, (2021). https://doi.org/10.1109/LPT.2021.3093584

14. S. Wang, J. Kuang, J. Li, Y. Luo, H. Lu, G. Hu, Chaos-based secure communications in a large community, Phys. Rev. E 66(6), 065202, (2002). https://doi.org/10.1103/PhysRevE.66.065202

15. S. Liu, N. Jiang, A. Zhao, Y. Zhang, K. Qiu, Secure optical communication based on cluster chaos synchronization in semiconductor lasers network, IEEE Access 8, 11872–11879, (2020). https://doi.org/10.1109/ACCESS.2020.2965960

16. Z. Wang, C. Song, A. Yan, G. Wang, Complete synchronization and partial anti-synchronization of complex Lü chaotic systems by the UDE-based control method, Symmetry 14(3), 517, (2022). https://doi.org/10.3390/sym14030517

17. G. M. Mahmoud, E. E. Mahmoud, Complete synchronization of chaotic complex nonlinear systems with uncertain parameters, Nonlinear Dyn. 62(4), 875–882, (2010). https://doi.org/10.1007/s11071-010-9770-y

18. A. Razminia, D. Baleanu, Complete synchronization of commensurate fractional order chaotic systems using sliding mode control, Mechatronics 23(7), 873–879, (2013). https://doi.org/10.1016/j.mechatronics.2013.02.004

19. H. Wang, G. Chai, S. Kang, Adaptive fixed-time anti-synchronization and synchronization control for Liu–Chen–Liu chaotic systems with actuator faults, Int. J. Adapt. Control Signal Process. 38(6), 2158–2177, (2024). https://doi.org/10.1002/acs.3799

20. M. M. Aziz, S. F. Al-Azzawi, Anti-synchronization of nonlinear dynamical systems based on Gardano's method, Optik 134, 109–120, (2017). https://doi.org/10.1016/j.ijleo.2017.01.026

21. X. Fu, L. Fu, H. I. Marrani, Synchronization and anti-synchronization of a novel fractional order chaotic system with an exponential term, Electrotehnica, Electronica, Automatica 70(2), (2022). https://doi.org/10.46904/eea.22.70.2.1108007

22. L. Xiao, L. Li, P. Cao, Y. He, A fixed-time robust controller based on zeroing neural network for generalized projective synchronization of chaotic systems, Chaos Solitons Fractals 169, 113279, (2023). https://doi.org/10.1016/j.chaos.2023.113279

23. N. Yadav, Pallav, H. Handa, Projective synchronization for a new class of chaotic/hyperchaotic systems with and without parametric uncertainty, Trans. Inst. Meas. Control 45(10), 1975–1985, (2023). https://doi.org/10.1177/01423312221150294

24. M. Jin, K. Sun, S. He, A novel fractional-order hyperchaotic complex system and its synchronization, Chin. Phys. B 32(6), 060501, (2023). https://doi.org/10.1088/1674-1056/acc0f6

25. S. Singh, S. Han, S. M. Lee, Adaptive single input sliding mode control for hybrid-synchronization of uncertain hyperchaotic Lu systems, J. Franklin Inst. 358(15), 7468–7484, (2021). https://doi.org/10.1016/j.jfranklin.2021.07.037

26. K. Sebastian Sudheer, M. Sabir, Hybrid synchronization of hyperchaotic Lu system, Pramana 73(4), 781–786, (2009). https://doi.org/10.1007/s12043-009-0145-1

27. J. G. Barajas-Ramírez, G. Chen, L. S. Shieh, Hybrid chaos synchronization, Int. J. Bifurcat. Chaos 13(5), 1197–1216, (2003). https://doi.org/10.1142/S021812740300714X

28. M. Hu, Z. Xu, R. Zhang, A. Hu, Adaptive full state hybrid projective synchronization of chaotic systems with the same and different order, Phys. Lett. A 365(4), 315–327, (2007). https://doi.org/10.1016/j.physleta.2007.01.038

29. X. Shi, Z. Wang, Hybrid projective synchronization of fractional-order extended Hindmarsh–Rose neurons with hidden attractors, Axioms 12(2), 157, (2023). https://doi.org/10.3390/axioms12020157

30. S. Wang, Y. Yu, M. Diao, Hybrid projective synchronization of chaotic fractional order systems with different dimensions, Physica A 389(21), 4981–4988, (2010). https://doi.org/10.1016/j.physa.2010.06.048

31. E. Wang, S. Yan, X. Sun, Q. Wang, Analysis of bifurcation mechanism of new hyperchaotic system, circuit implementation, and synchronization, Nonlinear Dyn. 111(4), 3869–3885, (2023). https://doi.org/10.1007/s11071-022-08034-w

32. Pallav, H. Handa, Adaptive sliding mode control for synchronizing chaotic systems under external disturbances and uncertainties: circuit implementation and analysis, Analog Integr. Circuits Signal Process. 125(2), 29, (2025). https://doi.org/10.1007/s10470-025-02489-8

33. V. K. Shukla, M. C. Joshi, P. K. Mishra, C. Xu, Mechanical analysis and function matrix projective synchronization of El-Nino chaotic system, Phys. Scr. 100(1), 015255, (2024). https://doi.org/10.1088/1402-4896/ad9c28

34. S. Mobayen, J. Mostafaee, K. A. Alattas, M. T. Ke, Y. H. Hsueh, A. Zhilenkov, A new hyperchaotic system: circuit realization, nonlinear analysis and synchronization control, Phys. Scr. 99(10), 105204, (2024). https://doi.org/10.1088/1402-4896/ad71fc

35. D. Khattar, N. Deo, M. Sirohi, A simple 5D autonomous hyperchaotic system: dynamical analysis, synchronization via adaptive integral sliding mode control, and circuit realization. Bol. Soc. Mat. Mex. 31, 85 (2025). https://doi.org/10.1007/s40590-025-00777-x

36. D. Khattar, N. Deo, M. Sirohi, On novel Hexa-compound combination synchronization over nineteen n-dimensional category-B chaotic systems and electronic circuit schematic, Phys. Scr. 100(1), 015280, (2024). https://doi.org/10.1088/1402-4896/ad9e3c

37. D. Khattar, N. Agrawal, M. Sirohi, Qualitative analysis of a new 6D hyper-chaotic system via bifurcation, the Poincaré notion, and its circuit implementation. Indian J. Phys 98(1), 259, (2024) https://doi.org/10.1007/s12648-023-02796-8

38. P. Li, R. Gao, C. Xu, Y. Li, Chaos suppression of a fractional-order modificatory hybrid optical model via two different control techniques, Fractal Fract. 6(7), 359, (2022). https://doi.org/10.3390/fractalfract6070359

39. H. Zhang, Z. Ding, L. Wang, Predefined-time multi-switch combination-combination synchronization of fractional-order chaotic systems with time delays, Phys. Scr. 99(10), 105223, (2024). https://doi.org/10.1088/1402-4896/ad7357

40. S. Yan, B. Zheng, J. Jiang, Adaptive multi-switching synchronization control of six-dimensional conservative systems based on memristor, Eur. Phys. J. Plus 139(9), 837, (2024). https://doi.org/10.1140/epjp/s13360-024-05610-4

41. D. Liu, T. Li, X. He, Fixed-time multi-switch combined–combined synchronization of fractional-order chaotic systems with uncertainties and external disturbances, Fractal Fract. 7(4), 281, (2023). https://doi.org/10.3390/fractalfract7040281

42. D. Khattar, M. Sirohi, R. Bansal, Comparative analysis of two novel chaotic systems, and validation of hybrid function projective and complete synchronization using active-adaptive control, Phys. Scr. 99(12), 125244, (2024). https://doi.org/10.1088/1402-4896/ad8e9a

43. M. Mohadeszadeh, N. Pariz, An application of adaptive synchronization of uncertain chaotic system in secure communication systems, Int. J. Model. Simul. 42(1), 143–152, (2022). https://doi.org/10.1080/02286203.2020.1848281

44. S. S. Nayyer, R. Gunjal, S. R. Wagh, N. M. Singh, Synchronization of uncertain chaotic systems with minimal parametric information, Physica D 460, 134059, (2024). https://doi.org/10.1016/j.physd.2024.134059

45. D. Khattar, N. Agrawal, M. Sirohi, Dynamical analysis of a 5D novel system based on Lorenz system and its hybrid function projective synchronisation using adaptive control, Pramana 97(2), 76, (2023). https://doi.org/10.1007/s12043-023-02544-x

46. P. P. Singh, A novel chaotic system with wide spectrum, its synchronization, circuit design and application to secure communication, Indian J. Sci. Technol. 14(28), 2351–2367, (2021). https://doi.org/10.17485/IJST/v14i28.103

47. S. Y. Al-hayali, S. F. Al-Azzawi, An optimal nonlinear control for anti-synchronization of Rabinovich hyperchaotic system, Indones. J. Electr. Eng. Comput. Sci. 19(1), 379–386, (2020). https://doi.org/10.11591/ijeecs.v19.i1.pp379-386

48. N. A. Saeed, H. A. Saleh, W. A. El-Ganaini, M. Kamel, M. S. Mohamed, On a new three-dimensional chaotic system with adaptive control and chaos synchronization, Shock Vib. 2023, 1969500, (2023). https://doi.org/10.1155/2023/1969500

49. P. Y. Dousseh, C. Ainamon, C. H. Miwadinou, A. V. Monwanou, J. B. Chabi Orou, Adaptive control of a new chaotic financial system with integer order and fractional order and its identical adaptive synchronization, Math. Probl. Eng. 2021, 5512094, (2021). https://doi.org/10.1155/2021/5512094

50. F. Hannachi, Analysis, dynamics and adaptive control synchronization of a novel chaotic 3-D system, SN Appl. Sci. 1(2), 158, (2019). https://doi.org/10.1007/s42452-019-0175-3

51. A. Roldán-Caballero, J. H. Pérez-Cruz, E. Hernández-Márquez, J. R. García-Sánchez, M. Ponce-Silva, J. D. Rubio, M. G. Villarreal-Cervantes, J. Martínez-Martínez, E. García-Trinidad, A. Mendoza-Chegue, Synchronization of a new chaotic system using adaptive control: design and experimental implementation, Complexity 2023, 2881192, (2023). https://doi.org/10.1155/2023/2881192

52. M. Sirohi, Qualitative analysis of a novel 5D chaotic system based on Bouali's system and its application in private communication via adaptive control, Bol. Soc. Mat. Mex. 29(1), 26, (2023). https://doi.org/10.1007/s40590-023-00497-0

53. J. L. Hindmarsh, R. M. Rose, A model of neuronal bursting using three coupled first order differential equations, Proc. R. Soc. Lond. B Biol. Sci. 221(1222), 87–102, (1984). https://doi.org/10.1098/rspb.1984.0024

54. N. Samardzija, L. D. Greller, Explosive route to chaos through a fractal torus in a generalized Lotka-Volterra model, Bull. Math. Biol. 50(5), 465–491, (1988). https://doi.org/10.1007/BF02458847

55. A. Wolf, J. B. Swift, H. L. Swinney, J. A. Vastano, Determining Lyapunov exponents from a time series, Physica D 16(3), 285–317, (1985). https://doi.org/10.1016/0167-2789(85)90011-9

56. S. L. Ross, Differential Equations, John Wiley & Sons, New York, (1984).

57. H. K. Khalil, Nonlinear Systems, Prentice Hall, (2002).

Dinesh Khattar,
Department of Mathematics,
Kirori Mal College, University of Delhi, Delhi-110007,
India.
E-mail address: dinesh.khattar31@gmail.com

and

Naokant Deo,
Department of Applied Mathematics,
Delhi Technological University, Delhi-110042,
India.
E-mail address: naokantdeo@dce.ac.in

and

Mukul Sirohi,
Department of Applied Mathematics,
Delhi Technological University, Delhi-110042,
India.
E-mail address: mukul7sirohi@gmail.com